Crack Detection Based on a Marked Point Process Model (Supplementary Material)

Jennifer Vandoni, Sylvie Le Hégarat-Mascle and Emanuel Aldea
SATIE - CNRS UMR 8029
Paris-Sud University, Paris-Saclay University, France
{jennifer.vandoni, sylvie.le-hegarat, emanuel.aldea}@u-psud.fr

I. Detailed results for selected test images

We provide full resolution images and detection results for four images presented in the article. The images have been selected as they cover a broad spectrum of characteristics:

- road images, in Fig. 1a, 1b, 1c which correspond to images 6005, 6036 and 6043 from the freely available CrackTree dataset [1]
- concrete wall, in Fig. 1d which correspond to image v003 from the Concrete dataset [2] which was kindly provided to us by the authors
- shadows, in Fig. 1a, 1b and 1d
- lane marker non-uniformities, in Fig. 1c
- filament cracks, in Fig. 1b and 1d
- complex/alligator patterns, in Fig. 1a and 1c

For each of the above images, we include, in this order (column-wise):

- the initial image
- the ground truth image (note that for the Concrete dataset the ground truth provided is dilated)
- the final result of our algorithm, as a separate binary image and also as a color image with the color code used in the paper in order to visualize it against the ground truth
- the binary image result of the NFA method used for comparison in the paper [3]

It is advised to zoom in the digital version of this document, in order to inspect the finer details of the detection results. Compared to the original document, the images presented below have a high resolution (and a much larger size).

References

[1] Q. Zou, Y. Cao, Q. Li, Q. Mao, and S. Wang, "Cracktree: Automatic crack detection from pavement images," *Pattern Recognition Letters*, vol. 33, no. 3, pp. 227–238, 2012.

[2] Y. Fujita and Y. Hamamoto, "A robust automatic crack detection method from noisy concrete surfaces," *Machine Vision and Applications*, vol. 22, no. 2, pp. 245–254, 2011.

[3] E. Aldea and S. Le Hégarat-Mascle, "Robust crack detection for unmanned aerial vehicles inspection in an a-contrario decision framework," *Journal of Electronic Imaging*, vol. 24, no. 6, pp. 061 119–061 119, 2015.

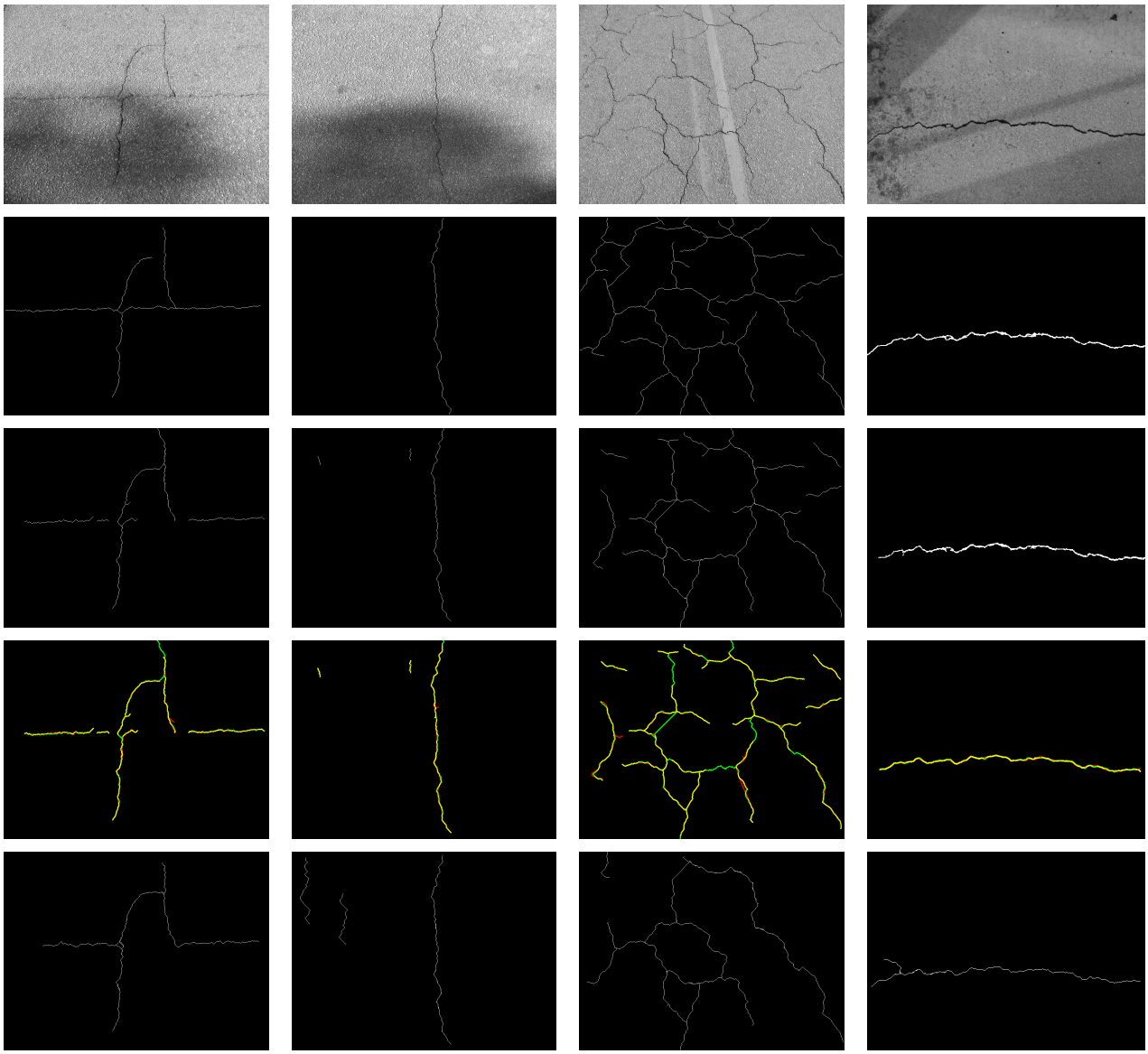

(a) (b) (c) (d)

Fig. 1. Results presented for different images (column-wise). First row: initial images. Second row: ground truth. Third row: final result of our algorithm as a binary image. Fourth row: final result of our algorithm, with the color code used in the main paper. Fifth row: final result of the NFA method used for comparison in the paper. The origin of the images is the following: (a) image 6005 of CrackTree dataset. (b) image 6036 of CrackTree dataset. (c) image 6043 of CrackTree dataset. (d) image v003 of Concrete dataset.